CHEMISTRY OF MATERIALS

ARTICLE

pubs.acs.org/cm

Size-Tunable, Ultrasmall $NaGdF_4$ Nanoparticles: Insights into Their T_1 MRI Contrast Enhancement

Noah J. J. Johnson,[†] Wendy Oakden,[§] Greg J. Stanisz,[§] R. Scott Prosser,[‡] and Frank C. J. M. van Veggel*[,†]

[†]Department of Chemistry, University of Victoria, P.O Box 3065, Victoria, British Columbia, Canada, V8W 3V6

[§]Department of Medical Biophysics, University of Toronto, Toronto, Ontario, Canada M5G 2M9

[‡]Department of Chemistry, University of Toronto, UTM, 3359 Mississauga Rd. North, Mississauga, Ontario, Canada, L5L 1C6

Supporting Information

ABSTRACT: We report on the size-tunable synthesis of thermodynamically stable (β) $NaGdF_4$ nanoparticles (NPs) below 10 nm. Paramagnetic β-$NaGdF_4$ NPs of four different sizes (2.5−8.0 nm with a narrow size distribution) were synthesized by simple modifications of the reaction conditions affecting nanoparticle growth dynamics. The synthesized NPs were transferred to water by exchanging the oleate ligands with biocompatible polyvinylpyrrolidone, and analyzed for their ability to affect magnetic resonance (MR) T_1 longitudinal relaxivity at 1.5 T. The ionic relaxivity (unit Gd^{3+} concentration) values increased from 3.0 mM^{-1} s^{-1} to 7.2 mM^{-1} s^{-1} with decreasing particle size, and the relaxivity of the 2.5-nm particle is almost twice that of clinically used Gd-DTPA (Magnevist) relaxivity. The relaxivity per contrast agent (i.e., per nanoparticle) for these NPs is 200−3000 times larger than the clinical agent, showing great potential as local contrast enhancement probes. The rate of increase in ionic relaxivity with decreasing NP size was similar to the rate of increase in the NP surface-to-volume (S/V) ratio, giving direct indication that the surface Gd ions are the major contributors to the relaxivity enhancement. Further analysis based on concentration of NPs, mass concentration of NP, and unit surface area, has revealed that the surface Gd ions on a larger NP affect the relaxivity more strongly than those on a smaller NP. This is discussed based on the increase in NP rotational correlation time (τ_R) with increasing size. A particular advantage of β-$NaGdF_4$ NPs over other Gd^{3+}-based inorganic NPs is that they are good hosts for upconverting emission. We demonstrate this by extending the synthesis protocol outlined here to prepare luminescent ultrasmall β- $NaGdF_4$:Yb^{3+}/Tm^{3+} NPs as potential bimodal probes.

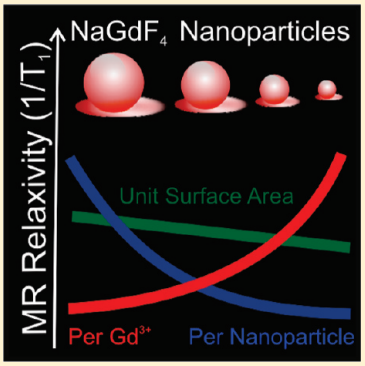

KEYWORDS: gadolinium nanoparticles, size-tunable, T_1 contrast agents, MRI, multimodal

INTRODUCTION

Colloidal nanomaterials show unique properties and are widely explored for a variety of applications.[1−4] Lanthanide-based nanomaterials have versatile utility in biological applications, as they can be made either as luminescent, magnetic, or as dual probe by selective doping of lanthanide ions.[5] In particular, paramagnetic Gd^{3+}-doped NPs show tremendous potential as contrast agents (CAs) for magnetic resonance imaging (MRI).[6,7] MRI is a powerful medical diagnostic tool, where the relaxation of water protons exposed to an external magnetic field is used to obtain morphological and anatomical information with unlimited tissue penetration and yet high spatial resolution.[8] CAs are used to improve the sensitivity, because they interact with the surrounding water protons and shorten their relaxation time to provide better contrast. Two types of CAs are clinically prevalent: (i) paramagnetic Gd^{3+} chelates, which affect the longitudinal relaxivity (r_1), and are termed positive (T_1) CAs, because they enhance the contrast;[9] and (ii) superparamagnetic iron oxide (SPIO) NPs, which affect transverse relaxivity (r_2) and are referred to as negative (T_2) CAs, because they diminish the signal intensity at the region of interest.[7,10] T_1 contrast agents are preferred over the T_2 agents as their enhanced brightening effect can easily be used to differentiate the signal from other pathogenic or biological conditions.[7]

Gd^{3+} chelates that are used clinically have very low body circulation time, because of their low molecular weight and show limitations as molecular probes for long-term tracking.[6] They also provide very low local contrast, because each chelate has only one Gd^{3+} ion. To increase the local contrast and relaxivity, second-generation agents have been developed by covalently anchoring Gd^{3+} chelates to different nanostructure frameworks,[11] or bundling multiple Gd^{3+} chelates together using polymers, dendrimers, liposomes, and viral capsids.[12] These structures have been shown to have high relaxivity and increased local contrast as multiple Gd^{3+} ions are coupled to a single nanostructure. The main disadvantage of this class of agents concerns their functionalization, which is tedious, expensive, and the number of ions that can be loaded to a NP is further limited by the number of anchoring sites available. Moreover, some of these aggregates are too large to be clinically useful.[6,7] Recently,

Received: May 6, 2011
Revised: July 8, 2011
Published: July 22, 2011

inorganic Gd^{3+}-doped NPs have been explored as a new class of T_1 CAs, partly because of their ease of synthesis, smaller size, and potential for improvement in contrast over currently used Gd^{3+} chelates. Other distinct advantages of this class of CAs are (i) dramatic increase in the local Gd ion concentration at the region of interest, (ii) ease of functionalization without compromising Gd^{3+} binding, (iii) increased tumbling time and consequent improvement in relaxivities, and (iv) control of targeting and clearance through their size.

Synthesis of inorganic Gd^{3+}-based NPs generally follows one of two protocols: (i) direct nanoprecipitation in water or polyol using a stabilizing agent which allows for crystal growth, followed by extraction and exchange with a more robust stabilizing agent;[13−18] (ii) preparation of hydrophobic NPs in high boiling organic solvents and subsequent transfer of the NPs into water using a hydrophilic ligand to render them water-soluble.[19−23] While the first approach is simpler and direct, synthetic methods employing high boiling organic solvents yield improved size control and uniformity.[24,25] Several studies have shown that the particle size is directly related to biodistribution, clearance rate,[26−28] and MRI contrast capabilities.[13] This fact imposes a restriction on the permissible polydispersity of the NPs used as CAs, if control over the aforementioned parameters is desired. Hence, NP-based CAs developed for clinical use are required to be highly monodisperse.

Inorganic Gd^{3+}-based NPs such as GdF_3,[14] Gd_2O_3[13,16−18] and $GdPO_4$,[29] have shown 2−3 fold higher ionic relaxivity (per Gd^{3+} ion) than clinical complexes. These NPs are synthesized in water or polyol solutions with poor size control, which limits their suitability for clinical usage. Moreover, there are differing views on the individual contributions of the core,[13,14] and surface ions[16] to the observed relaxivity enhancement, and a systematic study is required to resolve the issue. These concerns were clearly articulated in recent reviews by Hyeon et al., who stated "uniformly sized nanoparticles of gadolinium or related lanthanide compounds have not yet been demonstrated"[7] and "the synthesis of most materials has not been fully optimized yet, and the contrasting mechanisms of many of these materials still remains unclear".[6] Recently, inorganic Gd^{3+}-doped NPs synthesized in polyol/water medium were compared to understand the contrasting mechanism.[16] The compared samples were from different synthetic methods and polydisperse, and the relaxivity was measured at different magnetic field strengths. Such factors are known to affect the observed relaxivity and do not allow for a complete understanding of the relaxivity enhancement. Although such studies are informative, they provide only circumstantial evidence, rather than a direct one for the enhancement factor.

Theoretically, NPs <10 nm in size show a dramatic increase in the ratio of surface ions to core ions with decreases in size. Therefore, particles in this size regime are ideal for gaining insights into their relaxivity enhancement. NPs used for such study should also be uniform in size, shape, and phase (crystal structure), because these parameters can impact the observed relaxivity. However, there are no known reported procedures for size-tunable synthesis of lanthanide NPs meeting all these criteria below 10 nm.

In this report, the synthesis of lanthanide-based NPs meeting all of the above criteria is described. Monodisperse $NaGdF_4$ NPs 2.5−8.0 nm in size were synthesized by optimizing the reaction parameters associated with both the nucleation and growth phases in a high boiling binary solvent mixture. The nucleation was controlled by the concentration of the coordinating ligand (i.e., oleic acid), while the growth phase was tuned by the reaction time and temperature. The NPs coated with oleate ligands were transferred to water using polyvinylpyrrolidone (PVP), which is a highly biocompatible and water-soluble polymer[30] in order to evaluate the parameters responsible for T_1 contrast enhancement under aqueous conditions. T_1 relaxivity measurements were performed at 1.5 T, as a function of effective Gd^{3+} ion concentration to determine their ionic relaxivities. Further analysis of relaxivity values based on the mass of the NPs, concentration of NPs, and unit surface area were done to delineate the parameters affecting the observed relaxivity. The studies show that the relaxivity enhancement is governed by two distinct parameters: (i) the surface-to-volume (S/V) ratio (i.e., number of surface ions) and (ii) the rotational correlation time (τ_R) of the CA both counteracting along the size range.

As β-$NaGdF_4$ is one of the best known crystalline phase for upconversion emission,[31] upconverting NPs as small as 6 nm with a core−shell structure were developed as an integrated bimodal probe to demonstrate the versatility of these NPs.

EXPERIMENTAL SECTION

All chemicals were from Sigma−Aldrich, except sodium hydroxide, dichloromethane (DCM) (from ACP Chemicals), and ethyl ether (anhydrous), dimethylformamide (DMF), toluene (which were from Caledon Laboratories).

Synthesis of Ultrasmall β-$NaGdF_4$ Nanoparticles. Gadolinium chloride hexahydrate (1 mmol), oleic acid (4 mL) and octadecene (15 mL) were mixed together and heated to 140 °C under vacuum until a clear solution formed, after which the solution was cooled to room temperature. A solution of NaOH (2.5 mmol) and ammonium fluoride (4 mmol) in methanol (10 mL) was added dropwise to this and the mixture was stirred overnight (∼15 h). The reaction mixture was then heated at 70 °C to remove the methanol and placed under a gentle argon flow. Afterward, the solution was heated rapidly to the desired temperature (∼10 °C/min) and maintained for a constant time, depending on the desired NP size. Subsequently, the solution was cooled to room temperature and the NPs precipitated using ethanol, centrifuged (4500 rpm, Beckman Coulter Spinchron 15-rotor F0630), and washed twice with ethanol. The NPs were finally dispersed in 5 mL of toluene and centrifuged, and the supernatant was stored. (No modifications in purification steps were made for the synthesis described below.)

Synthesis of β-$NaYF_4$ and β-$NaGdF_4$ Nanoparticles. Yttrium chloride hexahydrate (1 mmol) for β-$NaYF_4$ synthesis, or gadolinium chloride hexahydrate (1 mmol) for β-$NaGdF_4$, was mixed with 6 mL of oleic acid and 15 mL of octadecene. Other reagents and reaction conditions were same as explained above, except that the reaction mixture was heated to 300 °C for 90 min. The NPs were precipitated, washed, and stored in 5 mL of toluene.

Synthesis of Upconverting Core−Shell β-$NaGdF_4$ Nanoparticles. Gadolinium chloride hexahydrate (0.75 mmol), ytterbium chloride hexahydrate (0.24 mmol), and thulium chloride hexahydrate (0.01 mmol) were mixed with oleic acid (4 mL) and octadecene (15 mL) and heated to 140 °C under vacuum until a clear solution was formed, after which the clear solution was cooled to room temperature. To this, a solution of NaOH (2.5 mmol) and ammonium fluoride (4 mmol) in methanol (10 mL) was added and the mixture was stirred overnight (∼15 h). The reaction mixture was then heated at 70 °C to remove the methanol and then placed under a gentle argon flow. Subsequently, the solution was heated to 270 °C (∼10 °C/min) and maintained at this temperature for 45 min. After this, the solution was cooled to room temperature and the NPs precipitated and washed with ethanol before storage in 5 mL of cyclohexane.

For the core−shell synthesis, gadolinium chloride hexahydrate (1 mmol), oleic acid (8 mL), and octadecene (15 mL) were mixed together and heated to 140 °C under vacuum until a clear solution formed, after which the clear solution was cooled to 80 °C. The cyclohexane dispersion of core NPs was injected and cyclohexane removed under continuous stirring. Subsequently, the solution was cooled to 50 °C and NaOH (2.5 mmol) and ammonium fluoride (4 mmol) in methanol (10 mL) were added and stirred for 2 h, followed by removing the methanol at 70 °C and the reaction mixture placed under a gentle argon flow. The temperature was increased to 270 °C (∼10 °C/min and maintained for 30 min. Subsequently, the solution was cooled to room temperature and the NPs precipitated and washed with ethanol before being dispersed in 5 mL of toluene.

Phase Transfer of Hydrophobic Nanoparticles to Water. Oleate-stabilized NPs were exchanged with polyvinylpyrrolidone (PVP-10) (molecular weight of MW = 10 000 g/mol) in DCM and dimethylformamide (DMF) solvent mixture. The amount of polymer for exchange was based on the NP size and calculated such that there were ∼60 PVP molecules per square nanometer of surface. After the exchange, the NPs coated with PVP-10 were dispersed in distilled water and dialyzed (Dialysis Membrane 25000 MWCO, Spectrum Laboratories) against water for 6 h. The water was changed every 2 h. The water from the dialyzed dispersion of NPs was removed by rotary evaporation (40 °C, P_{max} = 8 mbar) and the NPs were then redispersed in fresh deionized water for relaxivity measurements.

Characterization. Transmission electron microscopy (TEM) samples were drop cast on a Formvar carbon-coated grid (300 mesh Cu), air-dried and imaged. Low-resolution TEM images were obtained from a Hitachi H-7000 microscope operating at 75 kV and a JEOL JEM-1400 microscope operating at 80 kV. High-resolution (HR-TEM) images were from FEI Tecnai field-emission scanning transmission electron microscope at 200 kV. The size distribution was obtained from averaging a minimum of 50 NPs.

X-ray diffraction (XRD) patterns were collected with a resolution of 0.05° (2θ) and a scan speed of 1°/min, using a Rigaku Miniflex diffractometer with a Cr source (Kα radiation, λ = 2.2890 Å) operating at 30 kV and 15 mA. The average NP size was determined using the Scherrer equation for the single peaks at ∼25° (2θ) and ∼65° (2θ); the deviation in calculated crystallite size was less that ±0.2 nm for all cases.

Dynamic light scattering (DLS) measurements were done using Brookhaven Zeta PALS instrument with a 90Plus/BI-MAS Multi Angle Particle Sizing option, equipped with a 15 mW solid-state laser (658 nm). All data were obtained at a single scattering angle (90°) and averaged over five scans.

Inductively coupled plasma mass spectroscopy (ICP-MS) analysis was carried out using a Thermo X-Series II (X7) quadrupole ICP-MS to determine the Gd^{3+} ion concentration on the nanoparticle stock solution used for relaxivity measurements. The water dispersion of NPs were digested in concentrated nitric acid at 135 °C in sealed Teflon vials for 3 days and diluted with ultrapure water before analysis. Calibration was done by analyzing serial dilutions of a mixed element synthetic standard containing a known amount of gadolinium. Each sample, standard and blank, were spiked with indium (to a concentration of ∼7 ppb) as the internal standard to correct for signal drift and matrix effects. Accuracy was confirmed by analysis of a standard reference material (SLRS-4).

Magnetic resonance (MR) T_1 relaxation measurements at 1.5 T were performed using a clinical MRI scanner (GE Signa, GE Medical Systems, Milwaukee, WI) and a standard inversion recovery spin echo sequence, with a repetition time (TR) of 4000 ms, an echo time (TE) of 9 ms, and seven inversion recovery times (TI = 50, 104, 215, 444, 921, 1907, and 3950 ms); the field of view was 12 cm × 6 cm, and the image plane was 128 × 128 with a slice thickness of 5 mm, allowing simultaneous imaging of up to 50 vials (1.5 mL). The regions of interest were then drawn for each of the vials at TI = 3950 ms, and the signal containing an average of 20 voxels for each TI was evaluated. The signal-to-noise ratio was ∼200. The deviation was 1% on the measured relaxation times and the best linear fit was used to determine the relaxivity from the concentration dependent plot measured at four different concentrations. The error in the relaxivity values was estimated from the deviations in the linear fit.

Optical measurements were carried out using an Edinburgh Instruments Model FLS920 fluorimeter with a 980-nm laser diode (JDS Uniphase type 63-00342) coupled to a 100-μm core fiber as the excitation source. The output from the laser was collimated using a fiber coupler and a long band-pass filter (850 nm) was used on the excitation side and a short band-pass filter (900 nm) on the collecting end of the red-sensitive Peltier-cooled Hamamatsu R955 PMT detector. Both core and core−shell NPs in toluene (approximately equal number of NPs) were taken in a 1-cm path-length quartz cuvette and upconversion emission spectra measured at a resolution of 2 nm with the same laser power density (150 W cm^{-2}) and corrected for the instrument sensitivity.

RESULTS AND DISCUSSION

Size-Tunable, Ultrasmall β-$NaGdF_4$ Nanoparticles. Attempts to prepare β-$NaGdF_4$ NPs by following the synthetic protocol used for β-$NaYF_4$ NPs[32] yields particles that show both size and shape dispersity (see Figure S1 in the Supporting Information). The growth mechanism of β-$NaGdF_4$ NPs in oleic acid and octadecene significantly differs from that of the well-studied β-$NaYF_4$.[32−35] It is clearly evident that Ostwald ripening of NPs dominates when gadolinium salts are used instead of yttrium salts, following the $NaYF_4$ synthesis protocol. In order to tune the NP size and restrict Ostwald ripening, modified protocols to synthesize uniform β-$NaGdF_4$ have been described previously.[36−39] These protocols give access to NP sizes above 10 nm, and we discuss the parameters to obtain NPs <10 nm in size with high size tunability and uniformity. There are no known reports for such β-$NaLnF_4$ NP synthesis.

Based on the LaMer nucleation−growth model, the growth of uniform NPs is mainly governed by a temporally discrete nucleation stage and a controlled slow growth of the existing nuclei.[40] During NP growth, if the growth phase is fast or the nucleation stage is delayed (i.e., if nucleation and growth phases overlap), the resulting NPs are polydisperse and control over their size is hard to achieve. In a previous detailed study on the growth of $NaLnF_4$ NPs it has been shown that Ostwald ripening is dominant in the case of $NaGdF_4$ in oleic acid and octadecene binary solvent mixture and that the energy barrier between the nucleation and growth stages is relatively low.[35] This clearly shows that the nucleation and growth phase are highly overlapped in Gd^{3+}-based reactions. To tune the synthesis to uniform Gd^{3+}-based NPs with controllable sizes, the separation of these two phases should be an important criteria.

The process of nucleation is strongly dependent on the concentration of stabilizing agent (i.e., oleic acid) which is related inversely to the number of nuclei formed. It has been suggested that, when a large excess of oleic acid is present, fewer nuclei are formed and these nuclei grow very rapidly and indiscriminately, leading to polydisperse NPs.[41,42] Because $NaGdF_4$ NPs are known to grow faster,[35] the critical step should be to control the nucleation stage and enable enough nuclei formation to suppress the indiscriminate growth. Following this hypothesis, the concentration of oleic acid was systematically reduced to control nucleation with a simultaneous reduction of the reaction temperature to control the growth of those existing nuclei. Thus, when the ratio of oleic acid to gadolinium salt was

decreased from 19:1 to 13:1, at a decreased reaction temperature of 270 °C (300 °C is used for $NaYF_4$ synthesis), highly uniform NPs of 4.0 ± 0.3 nm were obtained. Increasing the number of nuclei formed during the nucleation stage results in an increased number of NP growing at the same time, directly resulting in the decrease of the NP size. Transmission electron microscopy (TEM) images of these particles (Figure 1) indicates that the size distribution is excellent, leading to the self-assembly of these NPs into a hexagonal close-packed structure on the carbon-coated copper grid. The presence of oleate ligands on the NP surface leads to an average interparticle distance of ~2.5 nm.

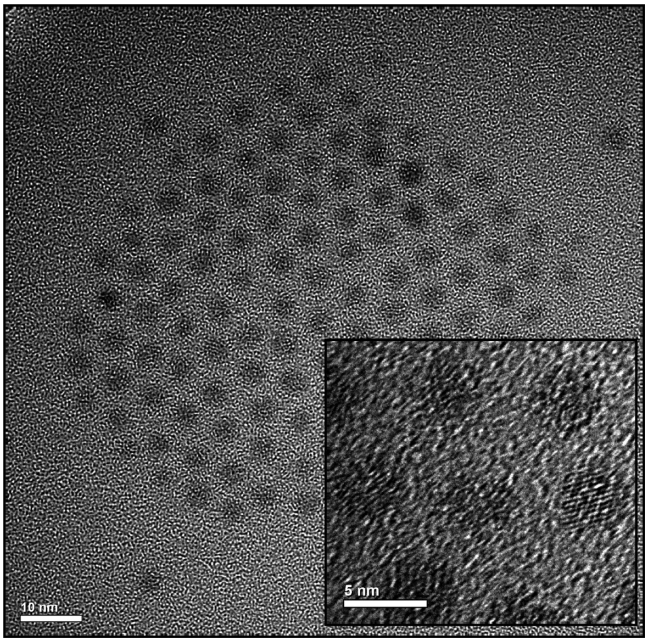

Figure 1. TEM image of 4.0 ± 0.3 nm oleate-stabilized $NaGdF_4$ NPs; inset shows the respective HR-TEM image.

By tuning the growth rate further, it was possible to achieve reproducibly monodisperse $NaGdF_4$ NPs of four sizes, viz., 2.5 ± 0.3, 4.0 ± 0.3, 6.5 ± 0.5, and 8.0 ± 0.5 (see Figure 2A−D and Figure S2 in the Supporting Information). The size of the NPs can precisely be controlled by careful choice of the reaction time and temperature, and these parameters are tabulated in Table 1. Powder X-ray diffraction (XRD) spectra of the NPs indicates that all the NPs are highly crystalline hexagonal-phase $NaGdF_4$. There was a regular, consistent broadening of the XRD peaks with decreasing NP size (see Figure 2E). The NP sizes calculated from the XRD peak widths using the Scherrer equation agree well with the sizes determined from TEM analysis. High-resolution TEM (HR-TEM) images shown in Figure 3 further confirms the crystalline nature of the NPs.

The synthesis outlined here using a simple modification of the reaction conditions not only allows for tunable NPs below 10 nm, but also yields the thermodynamically stable crystal structure (β-phase). This is in stark contrast to previous claims that such stable structures (β-phase) can only be synthesized above 10 nm.[35] There are no known reported procedures to make NPs <10 nm in size for this crystal phase, and this synthetic protocol allows for access to these size ranges with size tunability down to 2.5 nm.

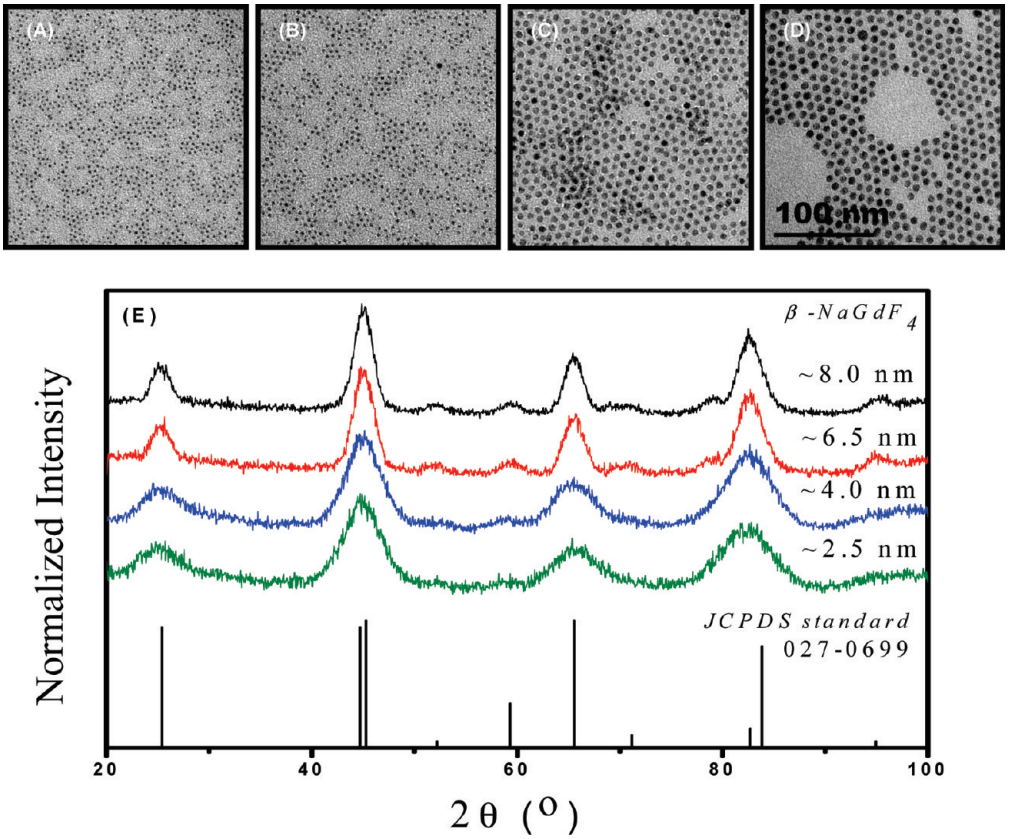

Figure 2. TEM images of oleate-stabilized $NaGdF_4$ NPs with sizes of (A) 2.5, (B) 4.0, (C) 6.5, and (D) 8.0 nm (scale bar is the same for all images), and (E) powder X-ray diffraction (XRD) pattern of the NPs (sizes are average numbers from TEM) overlaid with the reference pattern.

dx.doi.org/10.1021/cm201297x |*Chem. Mater.* 2011, 23, 3714–3722

Table 1. Parameters for Controlling the Growth Phase and the Size Distribution of NPs Obtained from TEM and XRD Analysis

temperature (°C)	time (min)	TEM size (nm)	XRD size (nm)
260	10	2.5 ± 0.3	2.6 ± 0.2
270	40	4.0 ± 0.3	3.8 ± 0.2
280	90	6.5 ± 0.5	7.2 ± 0.2
285	100	8.0 ± 0.5	8.1 ± 0.2

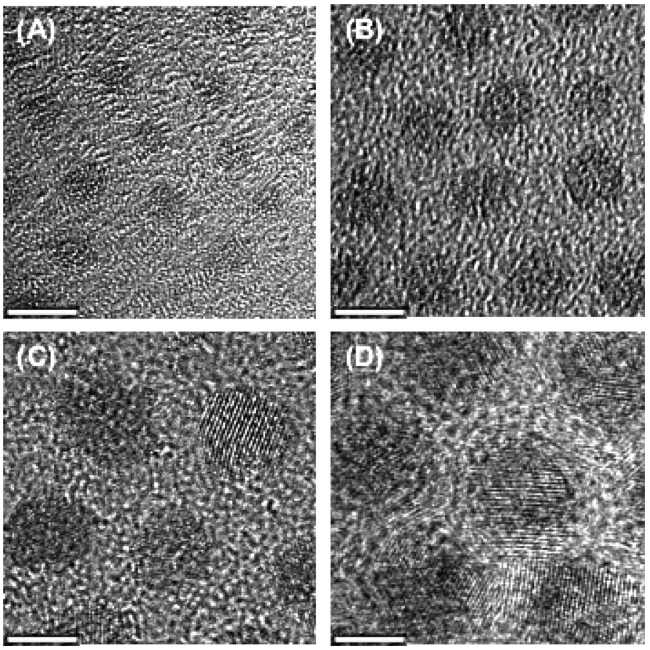

Figure 3. HR-TEM images of oleate-stabilized $NaGdF_4$ NPs (A-D) with sizes of (A) 2.5, (B) 4.0, (C) 6.5, and (D) 8.0 nm. Scale bar in all images is equal to 5 nm.

Surface Modification of β-$NaGdF_4$ Nanoparticles. The synthesized oleate-stabilized $NaGdF_4$ NPs were transferred from toluene to water by exchanging the oleate ligands with polyvinylpyrrolidone (PVP-10), following the exchange protocol that we recently published.[43] PVP is an ideal colloidal stabilizer for NP-based CAs, because of its high biocompatibility, nontoxicity, longer blood circulation times, and low accumulation in vital organs.[44,45] TEM and dynamic light scattering (DLS) analysis were performed to confirm that the particles had maintained their morphology and were not aggregated in water after exchange with PVP. The TEM images (see Figure S3 in the Supporting Information) show random distribution of individual NPs without any long-range ordering typically observed for the oleate-coated NPs. This is consistent with the fact that the oleates on the NP surface have been replaced with random coils of PVP. The hydrodynamic diameter measured by DLS (Figure 4) was between 10 nm and 17 nm for the four different core sizes with a low polydispersity in all cases. Considering PVP-10 with a hydrodynamic size of ~4 nm in water,[46] the observed DLS data further confirms that the NPs are coated with random coils of PVP chains.

Size-Dependent T_1 Relaxivity of $NaGdF_4$ Nanoparticles. The concentration-dependent T_1 relaxation of water protons at 1.5 T was determined for the aqueous dispersions of the four

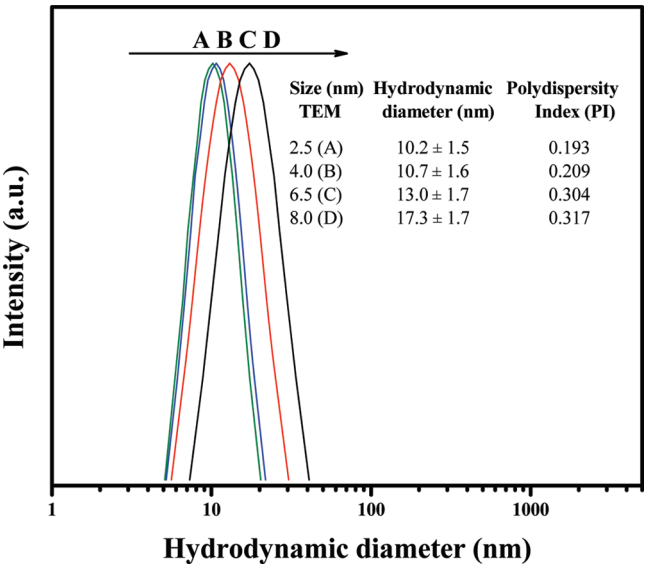

Figure 4. Dynamic light scattering (DLS) data showing the hydrodynamic diameter and polydispersity index for the phase-transferred $NaGdF_4$ NPs in water.

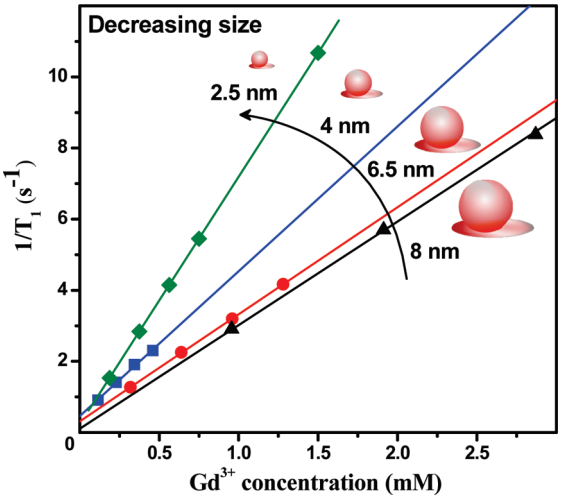

Figure 5. T_1 ionic relaxivity plot for $NaGdF_4$ NPs of different sizes in water (1.5 T) (where T_1 is the longitudinal relaxation time of water protons).

sizes of NPs prepared. To evaluate the ionic relaxivities, the gadolinium ion concentration of the NP dispersions was determined using ICP-MS, after digesting the NPs in concentrated nitric acid. The ionic relaxivity (r_1) (i.e., per Gd^{3+} ion concentration) was obtained from the slope of the linear regression fit from the relaxivity plots shown in Figure 5, and the values are tabulated in Table 2. The increase in slope corresponds to enhancement of the T_1 ionic relaxivity. Ionic relaxivities increase dramatically with decreasing particle size, from a value of 3.0 mM^{-1} s^{-1} for the 8.0-nm particles to 7.2 mM^{-1} s^{-1} for the smallest (i.e., 2.5 nm) particles. The clinical standard Gd-DTPA (Magnevist) has an ionic relaxivity of 3.7 mM^{-1} s^{-1} at 1.5 T.[8] While the ionic relaxivity for the larger 6.5- and 8.0-nm NPs are on par with the clinical CA, it is almost double that for the smallest particles. The relaxivity based on the mass concentration of NP (r_1/M), concentration of NPs or contrast

Table 2. Size-Dependent Relaxivity Data for $NaGdF_4$ NPs at 1.5 T

size (nm)	ionic relaxivity, $r_1/[Gd^{3+}]$ (mM^{-1} s^{-1})	mass relaxivity, r_1/M $(mg/mL)^{-1}$ s^{-1}	nanoparticle relaxivity, r_1/NP (mM^{-1} s^{-1})	surface area relaxivity, r_1/SA (ms^{-1})
2.5	7.2 ± 0.2	28	770	65
4.0	4.5 ± 0.2	18	2100	69
6.5	3.3 ± 0.2	13	6200	79
8.0	3.0 ± 0.2	12	11000	88

Table 3. Comparison of Ionic Relaxivity (r_1) Values of Uniformly Synthesized Gd^{3+}-Based NPs

nanoparticle	size (nm)	surface coating	r_1 (mM^{-1} s^{-1})	field (T)	ref
β-$NaGdF_4$	2.5	PVP	7.2	1.5	this work
α-$NaGdF_4$:Yb^{3+}:Er^{3+} /$NaGdF_4$ core/shell	20	PEG-phospholipid	1.40	1.5	21
α-$NaGdF_4$:Yb^{3+}:Er^{3+} /$NaGdF_4$ core/shell	41	PEG-phospholipid	1.05	1.5	21
β-$NaGdF_4$:Yb^{3+}:Er^{3+}	10	Octylamine-PAA	0.99	4.7	23
β-$NaGdF_4$:Yb^{3+}:Er^{3+}	40	Octylamine-PAA	0.47	4.7	23
β-$NaYF_4$:Yb^{3+}:Er^{3+}/ $NaGdF_4$ core/shell	28	Silica	0.48	3.0	20
Gd_2O_3 Yb^{3+}/Er^{3+} nanorods	2.5 * 18.0	Silane	1.5	9.4	22

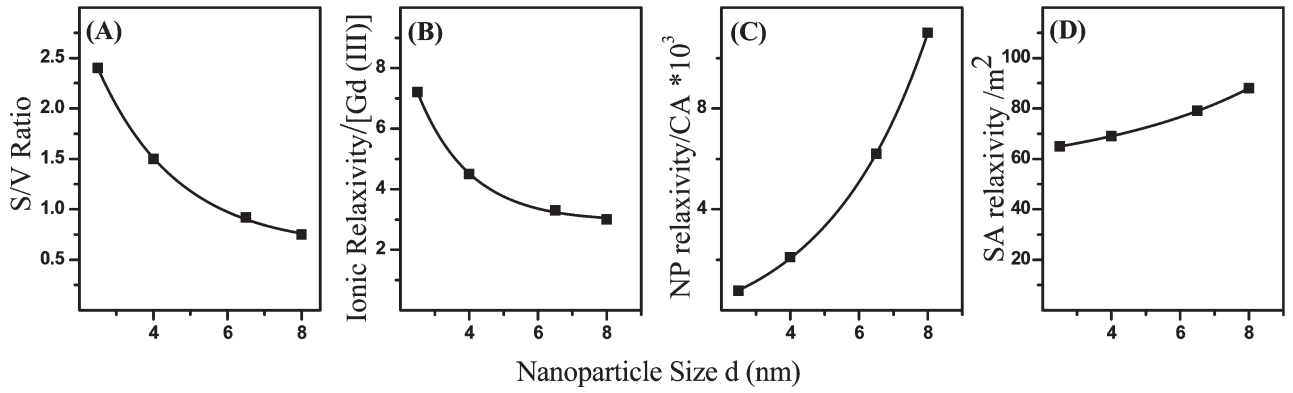

Figure 6. NP size-dependent plots of (A) the surface-to volume (S/V) ratio, (B) the ionic relaxivity, (C) the per-nanoparticle relaxivity, and (D) the relaxivity per square meter of surface area.

agent (r_1/NP), and unit surface area of NP (r_1/SA) were calculated from the ionic relaxivity ($r_1/[Gd^{3+}]$) (Table 2; see the Supporting Information for calculation), to further analyze the observed enhancement of ionic relaxivity with decreasing NP size.

The r_1/NP values correspond to per CA relaxivity and the relaxivity increases from 770 $mM^{-1}s^{-1}$ for the 2.5-nm particle to 11 000 $mM^{-1}s^{-1}$ for the 8.0-nm particles. Because the total number of Gd ions is higher in larger particles, the r_1/NP values increase with size. Clinical complexes typically contain one Gd^{3+} ion per CA, and their unit CA relaxivity is the same as their ionic relaxivity. Thus, the relaxivity offered by each $NaGdF_4$ NP described here is ∼200−3000 times that of clinical agents. This allows for enhanced local contrast while using NP-based CAs, which would be highly beneficial for targeted imaging. Moreover, bundling of multiple Gd ions in a crystalline NP affords rigid binding of the ions and leaching of Gd ions from the materials is less likely if they are stabilized with a protective ligand. ICP-MS analysis of the bulk water after dialysis of the NPs showed no appreciable amount of free Gd ions in solution, indicating that no leaching of ions from the NP occurred. The detection limit of the analysis for Gd ion concentration was ∼1.5 ng/L (∼10 pM). Thus, these NPs are good scaffolds for integrating multiple Gd ions without compromising on the Gd^{3+} binding.

The ability of contrast agents to be used as positive T_1 agents is governed by the ratio of their transverse relaxivity (r_2) to longitudinal relaxivity (r_1), and low r_2/r_1 ratios are considered to be ideal. The r_2/r_1 ratio for the smallest 2.5-nm NPs was ∼3.2 (see Figure S4 in the Supporting Information). Moreover, the relaxivity values for these ultrasmall NPs are much higher than the reported r_1 values of uniformly synthesized Gd^{3+}-based NPs developed to date, as summarized in Table 3. Note that we used a fairly long chain polymer (10 000 g/mol) for this study and a careful screening of ligands with shorter length to enhance water access to the surface ions may yield much better values for these NPs.

Analysis of T_1 Relaxivity Enhancement. The fraction of surface ions increases relative to the core ions with decreasing NP size, and there is a striking similarity in the dependence of NP S/V ratio and ionic relaxivity values with NP size (see Figures 6A and 6B). This signifies that the Gd ions on the surface are the major contributors toward the relaxation of water protons and Gd ions in the NP core do not show any significant effect toward relaxivity enhancement. To ensure that this, indeed, is the case,

dx.doi.org/10.1021/cm201297x |*Chem. Mater.* 2011, 23, 3714–3722

and to determine the extent to which Gd ions on the surface of differently sized NPs affect the relaxivity, the relaxivity per NP or contrast agent (r_1/NP), and the relaxivity per unit surface area of the NPs (r_1/SA) were analyzed (see Figures 6C and 6D, respectively). When the r_1/NP values are compared between the 2.5-nm and 8.0-nm particles, the 8.0-nm particles show a 14-fold relaxivity enhancement (770 mM^{-1} s^{-1} → 11 000 mM^{-1} s^{-1}) while the surface area increases only 10-fold (20 nm^2 → 200 nm^2). If surface ions on the NPs were contributing evenly toward the relaxivity enhancement, the increase in r_1/NP values should have a linear dependence with increase in NP surface area. This deviation is further substantiated by the relaxivity per unit surface area of the NPs (r_1/SA). If the Gd ions on the surface are the only contributors and affect the relaxivity uniformly, the r_1/SA should have remained the same, regardless of NP size (i.e., a straight line in Figure 6D). The r_1/SA values show an increasing trend with increase in NP size. In short, the surface Gd ions on a bigger NP affect the relaxivity more strongly than the surface Gd ions on a smaller NP.

These observations are comparable with results reported by Hyeon et al. on uniformly synthesized 20- and 41-nm α-$NaGdF_4$ NPs, which show a similar deviation in relaxivity values.[21] While the NP S/V ratio decreases by ~50% from the 20-nm particles to the 41-nm particles, the relaxivity values decrease only by ~25% (1.40 mM^{-1} s^{-1} and 1.05 mM^{-1} s^{-1} for the 20- and 41-nm particles, respectively). These observations suggest that other parameters play a role, even though less significant than the increase in the S/V ratio. We account for this deviation by analyzing other factors that are known to affect T_1 relaxivity.

The ability of a contrast agent to affect the relaxation of water protons can be classified into inner sphere (IS), secondary sphere (SS), and outer sphere (OS) contributions.[47] These individual contributions add up to the observed relaxivity (see eq 1).

$$r_1^{obs} = r_1^{IS} + r_1^{SS} + r_1^{OS} \quad (1)$$

The second and outer sphere contributions are mainly from the relaxation of water molecules hydrogen-bonded to the ligands and their exchange with bulk water. The ligands employed in our study for all the NPs are the same; hence, their outer sphere effects may be considered to be similar. Therefore, any difference in contribution from the outer shell may be neglected, and such assumptions have been used previously for similar Gd^{3+} complexes to understand the factors determining relaxivity enhancement.[48] The inner sphere contributions is dependent on the residence time of bound water (τ_M), the electron paramagnetic relaxation (T_{1e} and T_{2e}) and the molecular reorientation or the tumbling time of the contrast agent (τ_R). The first two factors, τ_M and $T_{1,2e}$, are frequency-dependent and their contributions are insignificant at low field strengths (0.5−1.5 T).[8,49] Therefore, the main contribution for the relaxivity at low field strengths is the tumbling time of the CA, and the second-generation CAs were developed based on this basic concept by anchoring the Gd^{3+} complexes to more slowly tumbling nanostructures. In short, more slowly tumbling CAs enhance the relaxivity of water molecules and at clinically relevant field strengths, tumbling times in the nanosecond time scale are said to be ideal.[11,50,51]

The tumbling time (τ_R) of spherical CAs can be deduced from the classical Debye−Stokes equation[50] (Calculation details are given in the Supporting Information.) The tumbling time of the NPs were calculated from the hydrodynamic radius determined by DLS and were found to be ~139, 161, 288, and 678 ns for the 2.5-, 4.0-, 6.5-, and 8.0-nm particles, respectively. Evidently, bigger NPs have longer tumbling times (τ_R), i.e., surface ions on bigger NPs tumble more slowly than on the smaller NPs. This fact accounts for the increase in r_1/SA values with increase in NP size. Gd^{3+} complexes coupled to different sizes of gold NPs have shown this effect,[52] and surface Gd ions on inorganic NPs can be visualized to be similar to one such structure.

To summarize: (i) relaxivity enhancement shows a clear dependence on the S/V ratio (i.e., the surface Gd ions, relative to the core ions, increase as the NP size decreases; hence, smaller NPs show high ionic relaxivity values, relative to the larger NPs); and (ii) the tumbling time (τ_R) increases as the NP size increases, counteracting the effect of the S/V ratio and making the surface ions on a larger NP affect the relaxivity more strongly than the ions on a smaller NP.

The enhancement of ionic relaxivity for the 2.5-nm particles over clinical complexes can be attributed to the difference in their tumbling times. The clinical complexes tumble on a picosecond time scale (Gd-DTPA ~54 ps),[53] while the 2.5-nm particles tumble on a nanosecond time scale (~139 ns). These findings, based on uniformly synthesized NPs, show that the previous suggestions of core Gd ions cooperatively enhancing the relaxivity,[13,14] and the cooperative effect of surface Gd ions,[16] are not the main factors affecting the relaxivity. There is a clear enhancement in relaxivity, because the number of surface ions increases, relative to core ions, as the NP size decreases and any contributions from core ions may be disregarded. The cooperative effect of surface Gd ions is also not a major factor, because, for a given unit surface area of NP, the relaxivity values should have remained the same, irrespective of their size.

Upconverting $NaGdF_4$ Core−Shell Nanoparticles. The synthesis of $NaGdF_4$ NPs presented here yields a thermodynamically stable hexagonal crystal phase, which is the best known matrix for upconversion emission to date.[31] Nanoparticles below ~10 nm in size are reported to have efficient body clearance;[54] previously reported sub-10-nm upconverting $NaLnF_4$ NPs were of α-phase (kinetic product),[55−57] and upconversion emission in

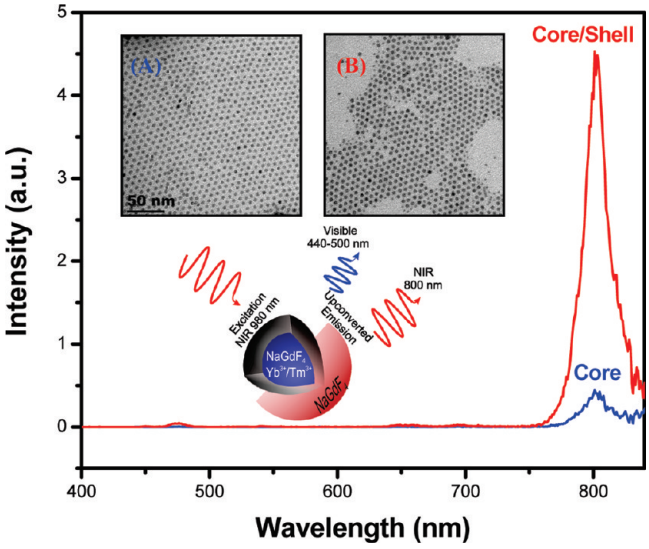

Figure 7. Upconversion emission spectra of $NaGdF_4$ Yb^{3+} (24%)/Tm^{3+} (1%) core and $NaGdF_4$ Yb^{3+} (24%)/Tm^{3+} (1%) core/undoped $NaGdF_4$ shell NPs in toluene excited with a 980-nm laser diode at 150 W cm^{-2}. (Inset: (A) TEM images of core and (B) core−shell NPs; scale bars are the same for both images.)

dx.doi.org/10.1021/cm201297x |Chem. Mater. 2011, 23, 3714–3722

this phase is an order of magnitude less than the β-phase. Using this synthetic route, β-$NaGdF_4$ NPs doped with Yb^{3+} and Tm^{3+} ions with a size of ~3.5 nm were synthesized, and the dopants did not hinder the formation of ultrasmall particles. When excited with a 980-nm diode laser, these NPs exhibit near-infrared (NIR) upconversion emission at 800 nm. Both the excitation and the emission peaks fall in the biological window, where biological tissues scatter the least, allowing for enhanced penetration depth. An undoped $NaGdF_4$ shell was grown on these upconverting NPs to enhance their emission efficiency and this resulted in the increase of NP size to ~6 nm. Similar core−shell NPs have been prepared and characterized rigorously in our laboratory,[19,58] and we expect that the case is also true for these structures. The emission intensity of the core−shell NPs increased 10-fold, compared to the core NPs (see Figure 7), which is consistent with other published works.[38,59,60]

CONCLUSIONS

We have presented a simple size-selective synthesis of paramagnetic $NaGdF_4$ nanoparticles (NPs) of four sizes, between 2.5 and 8.0 nm, that are applicable as MRI T_1 contrast agents. These NPs are the first evidence of size-tuned synthesis of uniform lanthanide-based particles <10 nm in size. This was accomplished by controlling the NP growth dynamics, such as the nucleation and growth rate. The amount of the coordinating ligand used in the synthesis was reduced to have increased nucleation and then the growth stage was controlled by carefully altering the reaction time and temperature. These NPs show effective shortening of the water proton T_1 relaxation rate, depending on their sizes, with the smallest 2.5-nm particles showing higher relaxivities, compared to clinical Gd^{3+} complexes. Correlations based on NP sizes and their relaxation rates show that the contributions from the surface-to-volume (S/V) ratio decrease with increasing particle size, while contributions from rotational correlation time (τ_R) increase with increasing size, with the S/V ratio being the dominant factor.

We also show that these NPs can be extended to other applications without compromising on their ultrasmall size by synthesizing ~6-nm upconverting NPs with a core−shell structure as a potential bimodal probe. In addition, the small size range presented allows for biological clearance issues to be addressed for this class of materials.

Finally, we expect that the relaxivity offered by these particles can be improved through judicious approaches such as confinement in nanoporous structures,[53] controlled aggregation,[61] and tuning of the surface ligands to allow enhanced water access, which will help to realize the true potential of these size-tunable NPs. Studies using modified surface transfer protocols to address water access to the surface ions and solvent-viscosity-dependent studies to better understand the effect of tumbling time are planned for these materials.

ASSOCIATED CONTENT

Supporting Information. Low-resolution TEM showing ensemble of NPs for oleate-stabilized and PVP-stabilized NPs, comparative TEM images of $NaYF_4$ and $NaGdF_4$ NPs, T_2 relaxivity plot, XRD spectra of core and core−shell upconverting NPs, and calculation details for relaxivity values. This material is available free of charge via the Internet at http://pubs.acs.org.

AUTHOR INFORMATION

Corresponding Author
*E-Mail: fvv@uvic.ca.

ACKNOWLEDGMENT

We thank the Natural Science and Engineering Research Council (NSERC), the Canada Foundation for Innovation (CFI), the British Columbia Knowledge Development Fund (BCKDF) of Canada for funding. We also acknowledge Dr. Jody Spence (University of Victoria) for the ICP-MS analysis.

REFERENCES

(1) Burda, C.; Chen, X. B.; Narayanan, R.; El-Sayed, M. A. *Chem. Rev.* **2005**, *105*, 1025–1102.
(2) De, M.; Ghosh, P. S.; Rotello, V. M. *Adv. Mater.* **2008**, *20*, 4225–4241.
(3) Pellegrino, T.; Kudera, S.; Liedl, T.; Javier, A. M.; Manna, L.; Parak, W. J. *Small* **2005**, *1*, 48–63.
(4) Shipway, A. N.; Katz, E.; Willner, I. *ChemPhysChem* **2000**, *1*, 18–52.
(5) Wang, F.; Liu, X. G. *Chem. Soc. Rev.* **2009**, *38*, 976–989.
(6) Na, H. B.; Hyeon, T. *J. Mater. Chem.* **2009**, *19*, 6267–6273.
(7) Na, H. B.; Song, I. C.; Hyeon, T. *Adv. Mater.* **2009**, *21*, 2133–2148.
(8) Bottrill, M.; Nicholas, L. K.; Long, N. J. *Chem. Soc. Rev.* **2006**, *35*, 557–571.
(9) Caravan, P.; Ellison, J. J.; McMurry, T. J.; Lauffer, R. B. *Chem. Rev.* **1999**, *99*, 2293–2352.
(10) Louie, A. *Chem. Rev.* **2010**, *110*, 3146–3195.
(11) Werner, E. J.; Datta, A.; Jocher, C. J.; Raymond, K. N. *Angew. Chem., Int. Ed.* **2008**, *47*, 8568–8580.
(12) Aime, S.; Castelli, D. D.; Crich, S. G.; Gianolio, E.; Terreno, E. *Acc. Chem. Res.* **2009**, *42*, 822–831.
(13) Bridot, J. L.; Faure, A. C.; Laurent, S.; Riviere, C.; Billotey, C.; Hiba, B.; Janier, M.; Josserand, V.; Coll, J. L.; Vander Elst, L.; Muller, R.; Roux, S.; Perriat, P.; Tillement, O. *J. Am. Chem. Soc.* **2007**, *129*, 5076–5084.
(14) Evanics, F.; Diamente, P. R.; van Veggel, F. C. J. M.; Stanisz, G. J.; Prosser, R. S. *Chem. Mater.* **2006**, *18*, 2499–2505.
(15) Hifumi, H.; Yamaoka, S.; Tanimoto, A.; Citterio, D.; Suzuki, K. *J. Am. Chem. Soc.* **2006**, *128*, 15090–15091.
(16) Park, J. Y.; Baek, M. J.; Choi, E. S.; Woo, S.; Kim, J. H.; Kim, T. J.; Jung, J. C.; Chae, K. S.; Chang, Y.; Lee, G. H. *ACS Nano* **2009**, *3*, 3663–3669.
(17) Ahren, M.; Selegard, L.; Klasson, A.; Soderlind, F.; Abrikossova, N.; Skoglund, C.; Bengtsson, T.; Engstrom, M.; Kall, P. O.; Uvdal, K. *Langmuir* **2010**, *26*, 5753–5762.
(18) Petoral, R. M.; Soderlind, F.; Klasson, A.; Suska, A.; Fortin, M. A.; Abrikossova, N.; Selegard, L.; Kall, P. O.; Engstrom, M.; Uvdal, K. *J. Phys. Chem. C* **2009**, *113*, 6913–6920.
(19) Abel, K. A.; Boyer, J. C.; van Veggel, F. C. J. M. *J. Am. Chem. Soc.* **2009**, *131*, 14644–14645.
(20) Guo, H.; Li, Z. Q.; Qian, H. S.; Hu, Y.; Muhammad, I. N. *Nanotechnology* **2010**, *21*, 125602.
(21) Il Park, Y.; Kim, J. H.; Lee, K. T.; Jeon, K. S.; Bin Na, H.; Yu, J. H.; Kim, H. M.; Lee, N.; Choi, S. H.; Baik, S. I.; Kim, H.; Park, S. P.; Park, B. J.; Kim, Y. W.; Lee, S. H.; Yoon, S. Y.; Song, I. C.; Moon, W. K.; Suh, Y. D.; Hyeon, T. *Adv. Mater.* **2009**, *21*, 4467–4471.
(22) Das, G. K.; Heng, B. C.; Ng, S. C.; White, T.; Loo, J. S. C.; D'Silva, L.; Padmanabhan, P.; Bhakoo, K. K.; Selvan, S. T.; Tan, T. T. Y. *Langmuir* **2010**, *26*, 8959–8965.
(23) Ryu, J.; Park, H. Y.; Kim, K.; Kim, H.; Yoo, J. H.; Kang, M.; Im, K.; Grailhe, R.; Song, R. *J. Phys. Chem. C* **2010**, *114*, 21077–21082.
(24) Parak, W. J.; Gerion, D.; Pellegrino, T.; Zanchet, D.; Micheel, C.; Williams, S. C.; Boudreau, R.; Le Gros, M. A.; Larabell, C. A.; Alivisatos, A. P. *Nanotechnology* **2003**, *14*, R15–R27.

(25) Park, J.; Joo, J.; Kwon, S. G.; Jang, Y.; Hyeon, T. *Angew. Chem., Int. Ed.* **2007**, *46*, 4630–4660.
(26) De Jong, W. H.; Hagens, W. I.; Krystek, P.; Burger, M. C.; Sips, A.; Geertsma, R. E. *Biomaterials* **2008**, *29*, 1912–1919.
(27) Pan, Y.; Neuss, S.; Leifert, A.; Fischler, M.; Wen, F.; Simon, U.; Schmid, G.; Brandau, W.; Jahnen-Dechent, W. *Small* **2007**, *3*, 1941–1949.
(28) Semmler-Behnke, M.; Kreyling, W. G.; Lipka, J.; Fertsch, S.; Wenk, A.; Takenaka, S.; Schmid, G.; Brandau, W. *Small* **2008**, *4*, 2108–2111.
(29) Hifumi, H.; Yamaoka, S.; Tanimoto, A.; Akatsu, T.; Shindo, Y.; Honda, A.; Citterio, D.; Oka, K.; Kuribayashi, S.; Suzuki, K. *J. Mater. Chem.* **2009**, *19*, 6393–6399.
(30) Rabin, O.; Perez, J. M.; Grimm, J.; Wojtkiewicz, G.; Weissleder, R. *Nat. Mater.* **2006**, *5*, 118–122.
(31) Krämer, K. W.; Biner, D.; Frei, G.; Güdel, H. U.; Hehlen, M. P.; Lüthi, S. R. *Chem. Mater.* **2004**, *16*, 1244–1251.
(32) Li, Z. Q.; Zhang, Y. *Nanotechnology* **2008**, *19*, 345606.
(33) Li, Z. Q.; Zhang, Y.; Jiang, S. *Adv. Mater.* **2008**, *20*, 4765–4769.
(34) Ye, X.; Collins, J. E.; Kang, Y.; Chen, J.; Chen, D. T. N.; Yodh, A. G.; Murray, C. B. *Proc. Natl. Acad. Sci. U.S.A.* **2010**, *107*, 22430–22435.
(35) Mai, H. X.; Zhang, Y. W.; Si, R.; Yan, Z. G.; Sun, L. D.; You, L. P.; Yan, C. H. *J. Am. Chem. Soc.* **2006**, *128*, 6426–6436.
(36) Liu, Y. S.; Tu, D. T.; Zhu, H. M.; Li, R. F.; Luo, W. Q.; Chen, X. Y. *Adv. Mater.* **2010**, *22*, 3266–3271.
(37) Naccache, R.; Vetrone, F.; Mahalingam, V.; Cuccia, L. A.; Capobianco, J. A. *Chem. Mater.* **2009**, *21*, 717–723.
(38) Wang, F.; Wang, J. A.; Liu, X. G. *Angew. Chem., Int. Ed.* **2010**, *49*, 7456–7460.
(39) Wang, F.; Han, Y.; Lim, C. S.; Lu, Y. H.; Wang, J.; Xu, J.; Chen, H. Y.; Zhang, C.; Hong, M. H.; Liu, X. G. *Nature* **2010**, *463*, 1061–1065.
(40) Murray, C. B.; Kagan, C. R.; Bawendi, M. G. *Annu. Rev. Mater. Sci.* **2000**, *30*, 545–610.
(41) Bullen, C. R.; Mulvaney, P. *Nano Lett.* **2004**, *4*, 2303–2307.
(42) van Embden, J.; Mulvaney, P. *Langmuir* **2005**, *21*, 10226–10233.
(43) Johnson, N. J. J.; Sangeetha, N. M.; Boyer, J. C.; van Veggel, F. C. J. M. *Nanoscale* **2010**, *2*, 771–777.
(44) Kaneda, Y.; Tsutsumi, Y.; Yoshioka, Y.; Kamada, H.; Yamamoto, Y.; Kodaira, H.; Tsunoda, S.; Okamoto, T.; Mukai, Y.; Shibata, H.; Nakagawa, S.; Mayumi, T. *Biomaterials* **2004**, *25*, 3259–3266.
(45) Robinson, S.; Williams, P. A. *Langmuir* **2002**, *18*, 8743–8748.
(46) Graf, C.; Vossen, D. L. J.; Imhof, A.; van Blaaderen, A. *Langmuir* **2003**, *19*, 6693–6700.
(47) Caravan, P.; Farrar, C. T.; Frullano, L.; Uppal, R. *Contrast Media Mol. Imaging* **2009**, *4*, 89–100.
(48) Caravan, P. *Acc. Chem. Res.* **2009**, *42*, 851–862.
(49) Aime, S.; Botta, M.; Terreno, E. *Adv. Inorg. Chem.* **2005**, *57*, 173–237.
(50) Caravan, P. *Chem. Soc. Rev.* **2006**, *35*, 512–523.
(51) Yang, J. J.; Yang, J. H.; Wei, L. X.; Zurkiya, O.; Yang, W.; Li, S. Y.; Zou, J.; Zhou, Y. B.; Maniccia, A. L. W.; Mao, H.; Zhao, F. Q.; Malchow, R.; Zhao, S. M.; Johnson, J.; Hu, X. P.; Krogstad, E.; Liu, Z. R. *J. Am. Chem. Soc.* **2008**, *130*, 9260–9267.
(52) Song, Y.; Xu, X. Y.; MacRenaris, K. W.; Zhang, X. Q.; Mirkin, C. A.; Meade, T. J. *Angew. Chem., Int. Ed.* **2009**, *48*, 9143–9147.
(53) Ananta, J. S.; Godin, B.; Sethi, R.; Moriggi, L.; Liu, X.; Serda, R. E.; Krishnamurthy, R.; Muthupillai, R.; Bolskar, R. D.; Helm, L.; Ferrari, M.; Wilson, L. J.; Decuzzi, P. *Nat. Nanotechnol.* **2010**, *5*, 815–821.
(54) Longmire, M.; Choyke, P. L.; Kobayashi, H. *Nanomedicine* **2008**, *3*, 703–717.
(55) Boyer, J. C.; Gagnon, J.; Cuccia, L. A.; Capobianco, J. A. *Chem. Mater.* **2007**, *19*, 3358–3360.
(56) Chen, G. Y.; Ohulchanskyy, T. Y.; Kumar, R.; Agren, H.; Prasad, P. N. *ACS Nano* **2010**, *4*, 3163–3168.
(57) Zhang, J.; Shade, C. M.; Chengelis, D. A.; Petoud, S. *J. Am. Chem. Soc.* **2007**, *129*, 14834–14835.
(58) Abel, K. A.; Boyer, J.-C.; Andrei, C. M.; van Veggel, F. C. J. M. *J. Phys. Chem. Lett.* **2011**, 185–189.
(59) Boyer, J. C.; Manseau, M. P.; Murray, J. I.; van Veggel, F. C. J. M. *Langmuir* **2010**, *26*, 1157–1164.
(60) Yi, G. S.; Chow, G. M. *Chem. Mater.* **2007**, *19*, 341–343.
(61) Cheung, E. N. M.; Alvares, R. D. A.; Oakden, W.; Chaudhary, R.; Hill, M. L.; Pichaandi, J.; Mo, G. C. H.; Yip, C.; Macdonald, P. M.; Stanisz, G. J.; van Veggel, F. C. J. M.; Prosser, R. S. *Chem. Mater.* **2010**, *22*, 4728–4739.